Oct 17th, 12:00 AM

Geometric Imperfections and Residual Stresses for Use in the Analytical Modeling of Cold-formed Steel Members

Benjamin W. Schafer

Teoman Pekoz

Thirteenth International Specialty Conference on Cold-Formed Steel Structures
St. Louis, Missouri U.S.A., October 17-18, 1996

GEOMETRIC IMPERFECTIONS AND RESIDUAL STRESSES FOR USE IN THE ANALYTICAL MODELING OF COLD-FORMED STEEL MEMBERS

Benjamin Schafer[1] & Teoman Peköz[2]

ABSTRACT

Geometric imperfections and residual stresses influence the behavior and ultimate strength of cold-formed steel members. Advanced analytical models (i.e. nonlinear finite element models) must reflect this by including appropriate geometric imperfections and residual stresses. To date, little has been done to summarize the existing literature on these topics. As a result, no consensus exists for what magnitudes or distributions should be used when including geometric imperfections and residual stresses in the analysis. In this paper existing literature is reviewed and a new series of measurements carried out with the goal of providing basic guidelines for the use of geometric imperfections and residual stresses in analytical models. The study results in promising methods for the measurement of imperfections, and shows that the existing literature can be used to at least partially realize the goal of using "practical inputs" in advanced analytical models.

1 INTRODUCTION

Finite element modeling of cold-formed steel members can be a daunting task. When loaded to ultimate strength cold-formed steel members typically exhibit a large post-buckling regime which is difficult to predict due to its sensitivity to input parameters and its relatively high degree of nonlinearity. Element selection, mesh discretization, boundary conditions, type of loading, geometric imperfections, residual stresses, and material models all influence the final results obtained by the analyst. The goal here is to examine two of these inputs: geometric imperfections, and residual stresses. Accurate modeling of geometric imperfections and residual stresses is important because they influence the ultimate load, and how that load is carried by the member.

[1]Graduate Research Assistant, Department of Civil and Environmental Engineering, Cornell University, Ithaca, New York
[2]Professor, Department of Civil and Environmental Engineering, Cornell University, Ithaca, New York

Despite the fact that many now seem to be undertaking finite element studies of cold-formed steel, little consensus has been reached as to what reasonable inputs are for the models. Given the power the analyst has, consistency across the field in the inputs would allow other researchers and practitioners to have more faith in the results. The goal here is to examine existing experimental data as well as perform additional experiments in order to make a first proposal on guidelines for analytical modeling of some aspects of cold-formed steel members.

2 GEOMETRIC IMPERFECTIONS

Geometric imperfections in cold-formed steel members refer to the deviations of an actual member from a "perfect" geometry. These imperfections include bowing, warping, or twisting of a member, as well as local imperfections such as dents, and plate waviness. It is not practical, nor is it generally required, to have a detailed understanding of the complete imperfection pattern existing in the member. The strength of a given cold-formed steel member is particularly sensitive to imperfections in the shape of its eigenmodes. If the amplitude of imperfections in the lowest eigenmodes is known, that information is sufficient to adequately characterize the most influential geometric imperfections. To this end, existing experimental data is gathered, and new experiments are conducted to make conclusions about what magnitude of imperfection analysts should be using.

2.1 Existing Experimental Data on Imperfections

A large number of researchers have investigated geometric imperfections of cold-formed steel members. Data was collected from experimental work completed by Bernard (1993), Dat and Peköz (1980), Ingvarsson (1977), Kwon (1992), Lau (1988), Mulligan (1983), and Thomasson (1978). Despite these investigations of geometric imperfections no attempt has been made to find any general characterization of geometric imperfections. In particular, much is left to be understood about the variation of plate imperfections along the length. An additional drawback to the cited research is that almost all of the data is for press-braked sections. Only the four deck sections tested by Bernard are roll-formed. In fact, the vast majority of the data is from lipped C-sections. However, all the researchers reported the maximum imperfections. Therefore, despite the limitations of the data one can get an overall view of the maximum geometric imperfections in cold-formed steel members.

2.1.1 Maximum Geometric Imperfections

As mentioned, the analyst is generally most concerned with imperfections that correspond to the eigenmodes of the member. Maximum imperfections can be used to provide conservative upper bounds for imperfection magnitudes of the eigenmodes of the member. These upper bound imperfection magnitudes can be used to determine lower bound strength predictions by the analyst. While it is true that larger imperfections do not always mean lower strength, if the maximum imperfections are used only for the magnitude of the lowest eigenmodes, the strength decreases as the magnitude of the imperfection increases. Of course, this use of the maximum imperfections is a simplification. In fact, since the maximum imperfections are not periodic along the length, using the maximum imperfection as a magnitude for the buckling shapes is quite conservative. Despite these

drawbacks, the maximum imperfections provide a reasonable criteria for a lower bound strength analysis.

For members in bending or compression two common buckling modes of importance are local buckling and distortional buckling; see for example: Kwon and Hancock (1992). The existing data on geometric imperfections from Bernard (1993), Dat and Peköz (1980), Ingvarsson (1977), Kwon (1992), Lau (1988), Mulligan (1983), and Thomasson (1978) is sorted in to two categories: (type 1) maximum local imperfection in a stiffened element, and (type 2) maximum deviation from straightness for a lip stiffened or unstiffened flange. The two imperfection types are illustrated in Figure 1. The data corresponding to the type 1 imperfection may be conservatively used as the imperfection magnitude for the local buckling mode. The type 2 measurements may be conservatively used as the imperfection magnitude for the distortional buckling mode. These approximations provide upper bound imperfection magnitudes for these two modes.

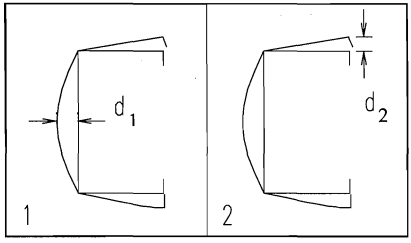

Figure 1 Definition of Geometric Imperfections

2.1.2 Predicting Type 1 Imperfections

The data for the type 1 imperfections in a stiffened element (as illustrated in Figure 1) is gathered and plotted in Figure 2 and Figure 3. The imperfection (d_1) is normalized by the plate thickness (t). In Figure 2, the imperfections are plotted against the plate slenderness - width divided by thickness (w/t). It is possible that due to the local nature of imperfections the dependence of the imperfection is due to the material thickness alone. This relationship is investigated in Figure 3. Neither Figure 2 nor Figure 3 provide a definitive explanation for the imperfection magnitudes, but both show certain trends which do exist in the data.

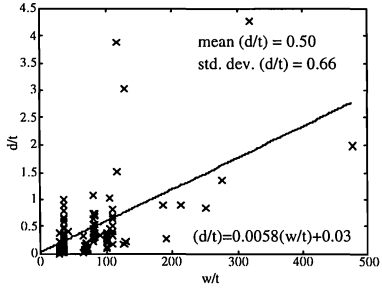

Figure 2 Element Slenderness vs. Normalized Type 1 Imperfection

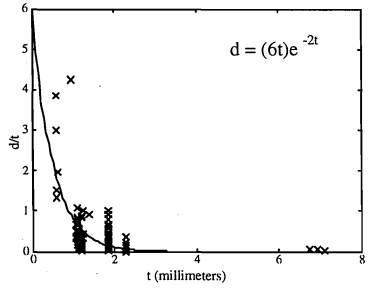

Figure 3 Material Thickness vs. Normalized Type 1 Imperfection

In order to provide some guidance on predicting the imperfection magnitudes simple equations based on the plots have been generated. In Figure 2, a best fit (least-squares) linear regression line is reported for the data. Simplifying that equation slightly, a coarse first approximation for the maximum imperfection based on Figure 2 is:

$$d_1 \approx 0.006w \qquad \textit{Eq 1}$$

Figure 3 shows an exponential curve that approximates the trend of the data. Based on this curve a second equation for predicting the maximum imperfection is proposed:

$$d_1 \approx 6te^{-2t} \qquad (d_1 \textit{ and } t \textit{ in } \textbf{\textit{millimeters}}) \qquad \textit{Eq 2}$$

$$d_1 \approx 152.4te^{-50.8t} \quad (d_1 \textit{ and } t \textit{ in } \textbf{\textit{inches}}) \qquad \textit{Eq 3}$$

2.1.3 Predicting Type 2 Imperfections

The type 2 imperfections in a unstiffened or lip-stiffened element (as illustrated in Figure 1) are examined in a manner similar to the type 1 imperfections. However, a plot for the material thickness versus the imperfection magnitude is excluded, because no trend exists in this plot for the type 2 imperfection. Figure 4 shows the element slenderness vs. the normalized type 2 imperfection. In Figure 4, Mulligan's results are circled to show the scatter found by one researcher for approximately the same slenderness. The tight group of results at a slenderness of 80 are all for another researcher: Kwon. This indicates that this imperfection is influenced largely by the manufacturer and not by the slenderness of the element. As a simple rule of thumb, the maximum deviation from straight, for elements with slenderness less than 80, is approximately equal to the plate thickness ($d/t = 1$). If one ignores any dependence on width or thickness and simply uses the average of the data, then the imperfection is approximately 1.8 millimeters or 0.07 inches.

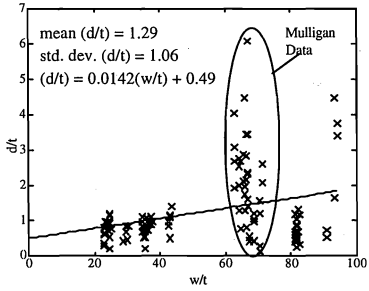

Figure 4 Element Slenderness vs. Normalized Type 2 Imperfection

2.1.4 Treating Maximum Geometric Imperfections as Random Variables

Another approach is to use the collected data and assume imperfections are random variables (see Schafer, Grigoriu, and Peköz 1996). This treatment ignores any dependence on the slenderness of the plate but allows one to more fully examine the influence of the

large variation that exists in imperfection data. Figure 5 shows the histogram for the type 1 imperfection and Figure 6 shows the histogram for the type 2 imperfection. The figures may also be used to select more conservative values for the imperfection magnitudes, rather than using the suggested equations.

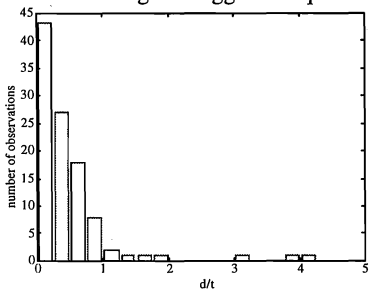

Figure 5 Histogram of Normalized Maximum Type 2 Imperfections

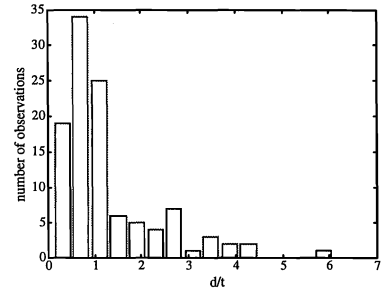

Figure 6 Histogram of Maximum Normalized Type 2 Imperfections

2.2 Measurement of Imperfections on a Typical Roll-Formed Member

The experimental data for geometric imperfections mentioned so far has distinct limitations. While the maximum deviation is of some interest as an upper bound, or perhaps as a descriptor of the worst "dents" in the member, they tell little about the average, or expected member imperfections. Also, since only a small amount of information is known about the deviation of the imperfections along the length - the existing data does not give a direct indication of the buckling modes which the imperfections might trigger. The existing data is also limiting, because no attempt has been made to generalize imperfection patterns - rather the imperfections of a particular member are always studied alone. In order to examine what if any periodicity exists in the imperfection of real cold-formed steel members an experimental program is undertaken for measuring these small magnitude imperfections. A method for carrying out this work is determined, and demonstrated on a roll-formed section used in practice.

2.2.1 Experimental Measurement of Local Geometric Imperfections

As an example, eleven nominally identical specimens are selected for study. The geometry of the specimens is shown in Figure 7. The thickness of the members (t = 0.9mm or 20 gauge) is relatively small, therefore these specimens are expected to exhibit measurable local geometric imperfections. Figure 8 illustrates the experimental setup that is used for the measurement of the local imperfections. The specimen is mounted on the table of a milling machine. This is done by laying the member flat on the milling table and then using vice grips to attach the section to two premounted angles. The milling table provides a flat reference surface for the measurement of the imperfections. The actual measurement is carried out by replacing the drill bit of the milling machine with a DCDT. This forms the basic mechanism for measuring the local imperfections. The procedure is automated

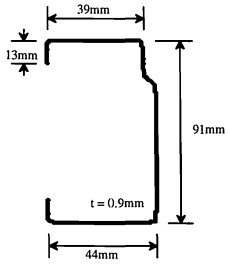

Figure 7 Nominal Geometry

through the use of the motor which drives the x direction motion of the milling table, and by gathering the data in a PC. The DCDT measurements are turned on and recorded in the computer at a constant rate. The milling table motor is then engaged. The table moves at a constant rate for a specified distance. Thus, since the sampling rate is constant, and the distance is known, then the distance between measurements is also known. This procedure is carried out on the top flange of 11 nominally identical specimens. For instance, the first plot of Figure 9 shows the imperfection deviation that was found along Specimen 3.

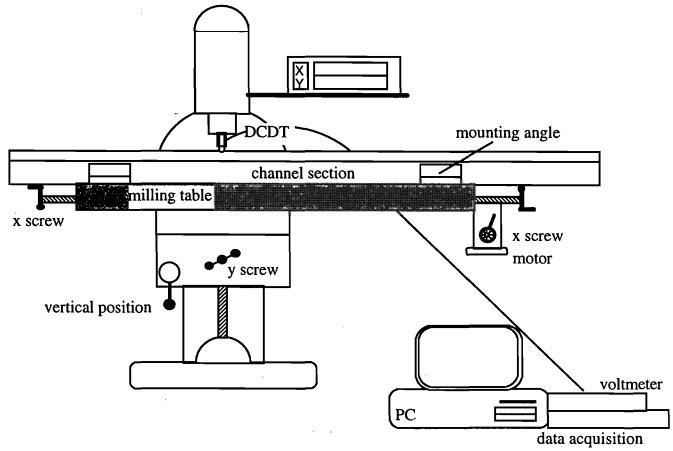

Figure 8 Experimental Setup

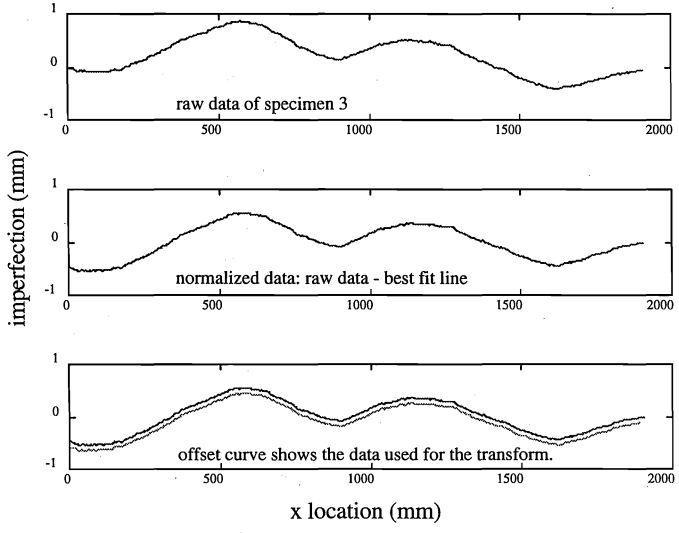

Figure 9 Imperfection Data for Specimen 3

2.2.2 Determination of Periodicity in the Imperfection "Signal"

The primary purpose of the experiment is to determine the local imperfections along the length of the member. This information allows any periodicity that exists in those imperfections to be investigated. Periodicity is important, because the eigenmodes of the member are characterized by certain wavelengths, or frequencies. In order to examine the periodicity of the imperfections a Fourier transform is used. The Fourier transform works on the principle that any function can be expressed as a summation of sine terms with an appropriate amplitude, frequency, and phase shift. To understand how the Fourier transform is used, an example is helpful. Assume that the third plot of Figure 10 corresponds to the imperfections along the length of some plate. This example imperfection is specially constructed as a superposition of two sine curves, as shown in the first two plots of Figure 10. A Fourier transform is performed on the imperfection "signal" and the result is the final plot of Figure 10. This plot has two distinct peaks, corresponding to the original two sine curves used to generate the imperfection. The transform reveals both the amplitude and frequency of the underlying sine curves. For an arbitrary imperfection pattern, peaks in the transform plot correspond to dominant sine waves in the original imperfection signal.

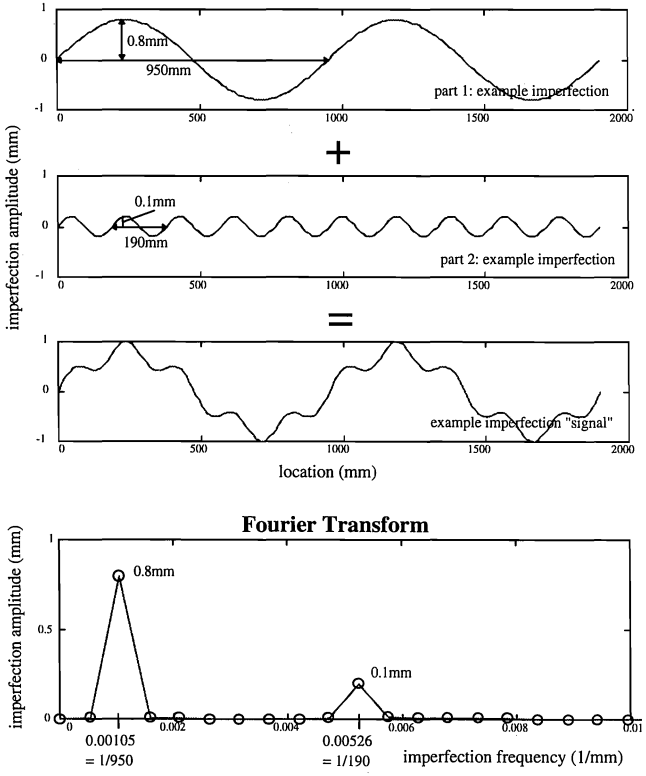

Figure 10 Example of the use of Fourier Transform

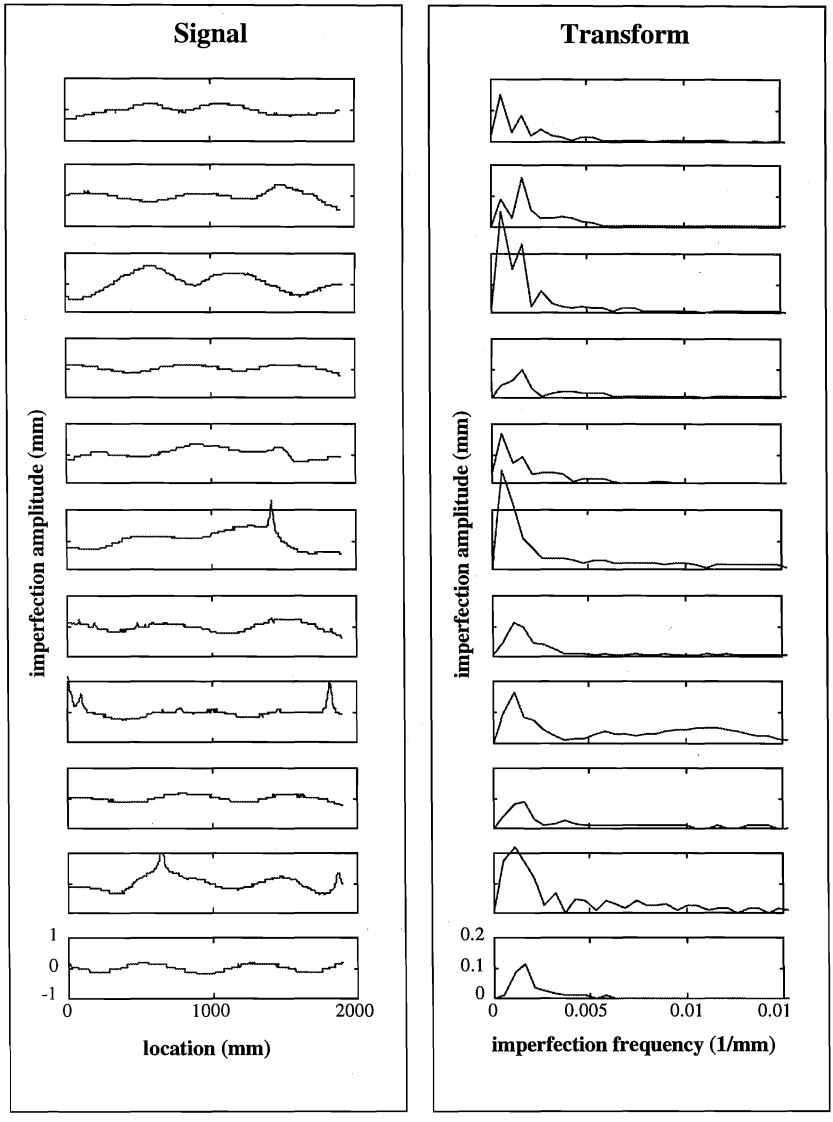

Figure 11 Imperfection Signal and Fourier Transform of 11 Specimens

2.2.3 Examination of Local Imperfection Experimental Results

In order to prepare the raw experimental data for comparisons, and for the Fourier transform, some post-processing is required. Figure 9 shows the post-processing of the data (in this case for Specimen 3) that is typical for this experiment. The imperfection quantity of interest is the deviation from perfect geometry. This deviation is found by determining a best-fit (least-squares) linear regression line for the raw data, and then subtracting this line from the raw data. The normalized data (the difference between the raw data and the regression line) is shown in the second plot of Figure 9. Further post-processing is required for the Fourier transform. It is desirable that the spacing of the measurements be equal for the 11 specimens. This insures that when comparing the Fourier transforms the same frequencies are compared from member to member. Since the original experimental data is sampled at slightly different rates, interpolation is needed to create an imperfection signal which is sampled at the same rate for all 11 specimens. The largest sampling rate used for the 11 specimens governs the sampling rate that is used in generating the Fourier transform. The final plot of Figure 9 again shows the normalized data, and in addition shows the same data sampled at the rate used in the transform, offset slightly from the original data for the purposes of comparison only.

In order to examine the periodicity of the data, Fourier transforms of the imperfection signals are completed. These transforms plot the imperfection frequency versus the imperfection amplitude. For instance, an imperfection frequency of $0.01mm^{-1}$ corresponds to an imperfection with a wavelength of 1/0.01 or 100mm (half-wavelength of 50mm). Figure 11 shows the imperfection signal and Fourier transform for all 11 specimens. Figure 11 readily allows comparison from specimen to specimen and from signal to transform. In examining the signals the spikes in specimens 6, 8 and 10 are most evident. These spikes correspond to visible dents in the top flange of those specimens. Except for the spikes, the imperfection signal is always within ±1mm. The Fourier transform of the 11 specimens more directly reveals the underlying structure. Despite the difference in the signals, the transforms all have relatively similar graphs: one or two low frequency peaks followed by little or no content after $0.005mm^{-1}$. This figure dramatically shows that periodicity does exist in the local imperfections of these members.

2.2.4 Characterizing Imperfections of Roll-Formed Specimens

The results of Figure 11 show the need for categorizing a general imperfection amplitude spectra for local imperfections of cold-formed steel members. As a first attempt at such an idea, the 11 transforms are averaged and used to create Figure 12. Figure 11 is an example of a curve that could be used to find the expected imperfection magnitude in any mode, or even generate a complete imperfection pattern. How would the spectra be used? For instance, say an elastic finite strip analysis (or any buckling analysis for that matter) indicates a sensitivity to modes with a half-wavelength of 500mm. This corresponds to an imperfection frequency of $[(500)(2)]^{-1} = 0.001mm^{-1}$. Examination of the inset of Figure 12 indicates an expected imperfection magnitude of approximately 0.11mm. Thus analytical modeling of the specimen should include the buckling mode with a 500mm half-wavelength at an amplitude of approximately 0.11mm. Of course this is only for the specimens analyzed, but the power of such a method is evident. Analytical models could

use imperfection patterns that are simple and realistic, thus improving the state of the art. Such "imperfection spectra" could be a powerful tool for the analyst.

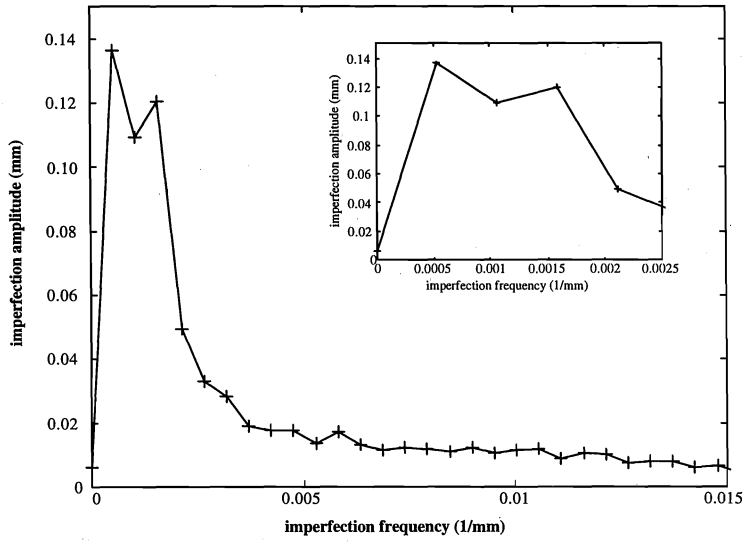

Figure 12 Average Imperfection Spectra

2.3 Proposed Guidelines for Modeling Imperfections

Up to this point the primary advice for imperfection magnitudes has been to use the value 0.1t (1% of the thickness). This value is thought to be large enough to avoid numerical problems that arise if imperfections are ignored, but small enough to allow other modes to contribute in the nonlinear analysis. In some regard this is still a reasonable guideline. However, a more practical approach for modeling imperfections is to use the bounds that the existing experimental data suggest. An eigenvalue analysis can be used to determine the imperfection distribution and the existing experimental data can be used to determine its magnitude. Of course, complete imperfection patterns such as Figure 12 suggests would be better, but they are still some time in coming. Thus if a limited amount of analysis is to be done, then for the imperfections, it is reasonable to get a lower bound strength by using the upper bound maximum imperfections only. More ambitious analysts may try to use the spectra of Figure 12 or treat the imperfections as random variables and conduct a Monte Carlo simulation using the data of Figure 5 and Figure 6.

Suggested Conservative Analysis - Distribution and Magnitudes:

Distribution: Use a shape which is dominated by the lowest buckling mode.

Magnitude: Use equations appropriate for the lowest mode.

Local Buckling: $d_1 \approx 6te^{-2t}$ (d_1 and t in mm) **or** $d_1 \approx 0.006w$

Distortional Buckling: $d_2/t = 0.014\,w/t + 0.5$ **or** $d_2 = 1.8$mm

Additional Analysis - Imperfection Magnitude and Distribution:

1. Use Figure 12, or generate other imperfection spectra to
   a) find the imperfection magnitude in critical modes **or**
   b) generate a complete imperfection distribution.
2. Conduct a Monte Carlo simulation for imperfections.

3 RESIDUAL STRESSES

The topic of residual stresses in cold-formed steel is particularly troublesome for the analyst. Inclusion of residual stresses in the model can be complicated. In addition, selecting an appropriate magnitude for the residual stresses is difficult due to a lack of data. As a result, residual stresses are often excluded from the model altogether, or the stress-strain diagram of the material is modified in an attempt to model the effect of residual stresses. While in some cases these approaches may be the only viable solution, it excludes an important behavioral aspect of cold-formed steel members. Cold-formed members are dominated by the flexural or through thickness variation of the residual stress. This variation of residual stresses leads to early yielding on the faces of cold-formed steel elements. This important aspect of the load carrying behavior of cold-formed material is completely lost without the inclusion of residual stresses.

3.1 Existing Experimental Data on Residual Stresses

In order to determine what distribution and magnitude of residual stresses should be used in modeling cold-formed steel, the work of Batista and Rodrigues (1992), Bernard (1993), Dat and Peköz (1980), Ingvarsson (1977), Key and Hancock (1993), Kwon (1992), and Weng (1987) are gathered and examined. The body of work covers both press-braked (PB) and roll-formed (RF) specimens. Table 1 shows the researchers and the type of specimens they examined.

Table 1 Summary of Specimen Type for Researchers

Researcher	***RF***	***PB***
Batista and Rodrigues	2	1
Bernard	3	3
Dat	2	2
Ingvarsson	0	2
Key	1	0
Kwon	0	2
Weng	8	3
	16	13

The data is further broken down into the different elements where the residual stresses are measured. The four selected areas are: corners, edge stiffened element (i.e. flange of a "C"), lips (i.e. the edge stiffener itself), and stiffened elements (i.e. web of a "C", flange of a "hat"). Table 2 shows the number of measurements at each location and what forming method was used to make the specimens.

Table 2 Location of Residual Stress Measurements

Researcher	***RF***	***PB***
Corners	24	15
Edge stiffened element	36	71
Lip	8	4
Stiffened element	83	55
	151	148

The residual stresses themselves are broken down into two types: flexural and membrane. Figure 13 shows the types of residual stresses considered. This breakdown can be misleading because analytical models usually have more complex distributions, but since the only experimental measurements are at the faces, the breakdown seems reasonable, if not wholly justified. The data for residual stresses is presented either as a percentage of the yield stress (%Fy) or as a ratio of residual stress to yield stress (Fr/Fy). With the data thus organized a proper investigation of residual stresses in cold-formed steel members can be made.

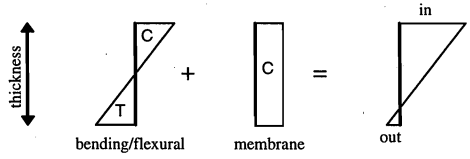

Figure 13 Definition of Flexural and Membrane Residual Stress

3.1.1 Membrane Residual Stresses

In order to examine the data on membrane residual stresses, histograms and a statistical summary are provided. Figure 14 and Figure 15 show histograms of the collected data for the membrane residual stress in roll-formed and press-braked members respectively. Table 3 shows the results for the membrane residual stress as a %Fy broken down by location in the cross-section. At first glance the histograms seem to indicate that the membrane residual stress is essentially zero. Examination of Table 3 shows this to be only partially true. The membrane residual stress for corners, and for lips of roll-formed members, appear significant. In addition, the membrane residual stresses are more prevalent in the roll-formed members. Thus analysis which ignores all membrane residual stresses may be an oversimplification (albeit a slight one.)

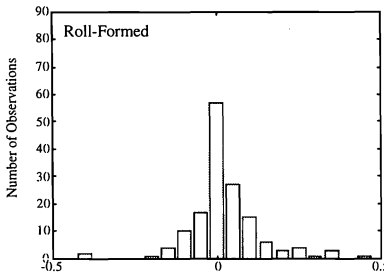

Figure 14 RF Membrane Residual Stress (Fr/Fy)

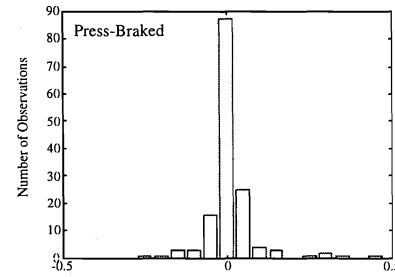

Figure 15 PB Membrane Residual Stress (Fr/Fy)

Table 3 Membrane Residual Stress as %Fy

	RF		***PB***	
	mean	*variance*	*mean*	*variance*
Corners	6.76	1.06	5.24	0.44
Edge Stiffened	3.87	1.02	0.90	1.03
Lip	7.86	1.50	0.25	0.28
Stiffened	-1.7	1.24	0.88	0.14

3.1.2 Flexural Residual Stress

Flexural, or bending, residual stresses are the most important component of the residual stress. They introduce the through thickness variation of residual stress in the material that proves significant in the analysis. In addition, the magnitude of the flexural residual stresses can be quite large, measured residual stresses equal to 50%Fy are not uncommon. In addition to large magnitude, the measured flexural residual stresses show a large amount of variation. The calculated mean and variance for the flexural residual stress broken down by location in the cross-section is reported in Table 4. The histograms of the flexural residual stress are shown in Figure 17. Figure 17 clearly shows the difficulty in characterizing residual stress by its mean alone. For edge stiffened elements the mean of the data is a relevant statistic, but what about for the corners? Despite these shortcomings, an analyst can not generally afford to do a series of analyses with different residual stresses, so one is left with the averages. Average values for both roll-formed and press-braked sections are shown graphically in Figure 16. The figure highlights the differences between roll-formed and press-braked sections, as well as showing the variation around the section. For a more conservative approximation of the residual stresses, the histograms (Figure 17) can be used to estimate the probability that a selected residual stress value will occur.

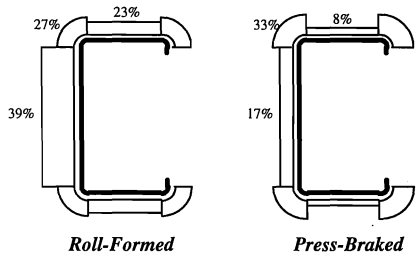

Figure 16 Average Bending Residual Stress as %Fy

Table 4 Flexural Residual Stress as %Fy

	RF		***PB***	
	mean	*variance*	*mean*	*variance*
Corners	26.84	5.00	32.71	3.30
Edge Stiffened	23.47	1.00	8.05	2.47
Lip	6.72	6.38	55.95*	11.65
Stiffened	38.92	6.21	16.89	4.48

* Some lips are flame-cut, thus distorting this value.

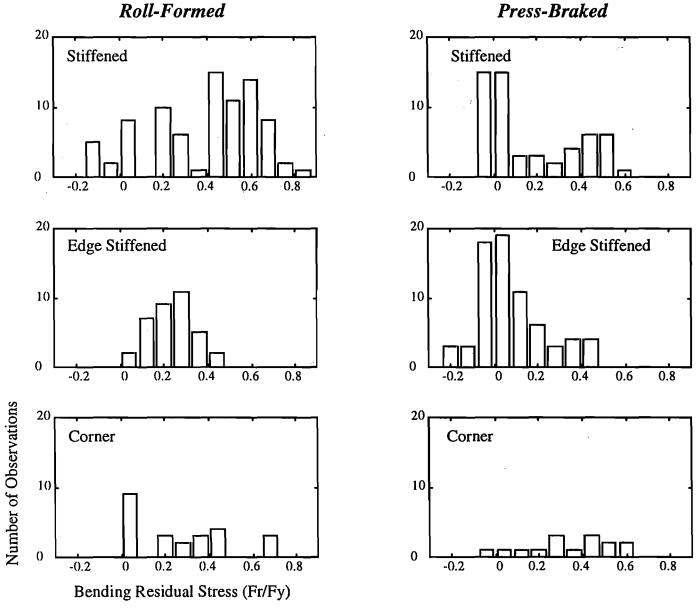

Figure 17 Histograms for Flexural Residual Stress

3.1.3 Press-Braked versus Roll-Formed

Due to the nature of residual stresses it seems quite reasonable to assume that press-braked sections and roll-formed sections have different residual stresses. This assumption is borne out by the collected data. Table 5 presents the mean and variance for all the collected data for roll-formed and press-braked specimens. It is clear, that residual stresses are significantly higher in roll-formed members.

Table 5 Summary Statistics RF vs. PB

	RF	***PB***
mean	0.3161	0.1502
variance	0.0552	0.0443
sample size	151	148

3.2 Proposed Guidelines for Modeling Residual Stresses

Figure 17 demonstrates that even in the cases where a fair amount of existing data can be found, a deterministic value for residual stress magnitudes is difficult to determine. A few points one can make with certainty are: that residual stresses are larger in roll-formed members, and that membrane residual stresses are quite small. These are not new conclusions; rather, the tests have borne out the assumptions most already make. Thus the analyst is left to treat residual stresses in a rather crude manner. Using Figure 16 and assuming that the membrane residual stresses are zero is a reasonable assumption if only one analysis is to be conducted. The histograms on Figure 17 could be used to select more conservative values for the residual stress magnitude.

Suggested Analysis - Residual Stress Magnitude and Distribution:

Distribution: Assume flexural residual stress only.

Magnitude: Use the appropriate values from Figure 16.

Additional Conservative Analysis - Residual Stress Magnitude and Distribution:

Distribution: Include a composition of flexural and membrane residual stress.

Magnitude: Use Figure 17 to select conservative values.

4 CONCLUSIONS

A great deal of complexity is required for the analytical modeling of the ultimate strength of cold-formed steel members. Comparison of results among analysts, as well as the usefulness of the analytical results requires a greater consensus on the inputs used in the modeling process. To this end, geometric imperfections and residual stresses are examined with the hope of determining practical distributions and magnitudes for their use in cold-formed steel modeling. Conservative bounds for imperfection magnitudes are established through an examination of the existing literature. The resulting equations for the imperfection magnitudes are limited, but do provide some characterization of imperfection magnitudes. A better approach is demonstrated experimentally. Eleven nominally identical specimens are shown to have periodicity in the local imperfections measured on the top flange. This method shows that characterizing geometric imperfections by an imperfection spectra may be a useful tool for future analysts and researchers. Examination of existing data on residual stresses once again demonstrates the difficulty in understanding the magnitude and distribution of residual stresses. Nonetheless, it is possible to provide some

insight into what values should be selected. The average flexural residual stresses are suggested for normal use in modeling residual stresses. While it is certainly true that much more needs to be done in this area, the authors hope that this paper will begin a discussion on more accurate and consistent inputs used in the analysis of cold-formed steel members.

5 REFERENCES

Batista, E. de M., Rodrigues, F.C. (1992). "Residual Stress Measurements on Cold-formed Profiles." *Experimental Techniques*, 16(5), 25-29.

Bernard, E.S. (1993). Flexural Behavior of Cold-Formed Profiled Steel Decking. Ph.D. Thesis, University of Sydney, Sydney, Australia.

Dat, D.T., Peköz, T.P. (1980). "The Strength of Cold-Formed Steel Columns." *Department of Structural Engineering*, School of Civil and Environmental Engineering, Cornell University, Report No. 80-4, Ithaca, New York.

Ingvarsson, L. (1977). "Cold-Forming Residual Stresses and Box Columns Built Up By Two Cold-Formed Channel Sections Welded Together." *Bulletin of The Department of Building Statics and Structural Engineering*, 121, The Royal Institute of Technology, Stockholm, Sweden.

Kwon, Y.B., (1992). Post-Buckling Behavior of Thin-Walled Channel Sections. Ph. D. Thesis, University of Sydney, Sydney, Australia.

Kwon, Y.B., Hancock, G.J. (1992). "Strength Tests of Cold-formed Channel Sections Undergoing Local and Distortional Buckling", *ASCE Journal of Structural Engineering*, 118(7).

Lau, S.C.W. (1988). Distortional Buckling of Thin-Walled Columns. Ph.D. Thesis, University of Sydney, Sydney, Australia.

Mulligan, G.P. (1983). The Influence of Local Buckling on the Structural Behavior of Singly Symmetric Cold-Formed Steel Columns. Ph.D. Thesis, Cornell University, Ithaca, New York.

Schafer, B.W., Grigoriu, M., Peköz, T. (1996). "A Probabilistic Examination of the Ultimate Strength of Cold-Formed Steel Elements." *Thirteenth International Specialty Conference on Cold-Formed Steel Structures*, St. Louis, Missouri.

Thomasson P. (1978). "Thin-Walled C-Shaped Panels in Axial Compression." Swedish Council for Building Research, D1:1978.

Weng, C.C. (1987). Flexural Buckling of Cold-Formed Steel Columns, Ph.D. Thesis, Cornell University, Ithaca, New York.